Experimental Determination of Third-Order Elastic Constants of Diamond

J. M. Lang, Jr. and Y. M. Gupta

Institute for Shock Physics and Department of Physics, Washington State University, Pullman, Washington 99164, USA
(Received 16 November 2010; published 22 March 2011)

To determine the nonlinear elastic response of diamond, single crystals were shock compressed along the [100], [110], and [111] orientations to 120 GPa peak elastic stresses. Particle velocity histories and elastic wave velocities were measured by using laser interferometry. The measured elastic wave profiles were used, in combination with published acoustic measurements, to determine the complete set of third-order elastic constants. These constants represent the first experimental determination, and several differ significantly from those calculated by using theoretical models.

Understanding the properties of carbon allotropes under conditions of high pressure is critical for studying the interiors of giant planets [1–3], the development of inertial confinement fusion [4], and in understanding carbon nanostructures [5]. Diamond, in particular, has widespread scientific and technological importance due to its exceptional mechanical, optical, and thermal properties [6]. Diamond anvil cells are routinely used to create static pressure conditions in excess of 300 GPa [7]. A recent study has suggested that the Raman spectra of diamond microcrystals may be used as a pressure standard up to 270 GPa [8]. Shock wave [9–11] and ramp wave [12] compression studies have explored the phase diagram of diamond up to 1 TPa. At these extreme conditions, the anharmonic properties of the diamond lattice play a central role in governing the thermomechanical and anisotropic response.

Third-order elastic constants (TOECs) reflect the lowest-order anharmonic response of a crystal and, as such, serve as a starting point for modeling the high stress response, developing ion-electron pseudopotentials [13] or empirical interatomic potentials [14], and studying properties of strained quantum wells [15] and physical phenomena related to lattice anharmonicity in general. In addition, third- and higher-order elastic constants provide a convenient approach to quantify the nonlinear elastic response of a solid [16]. Despite the importance of diamond and its widespread use in high pressure science, something as fundamental as the complete set of TOECs has not been determined experimentally. In large part, the exceptional mechanical properties of diamond, a cubic crystal, have made this determination difficult. Here, we show how this difficulty can be overcome and present an experimental determination of the six independent TOECs for diamond.

The pressure derivatives of the second-order elastic constants of diamond have been measured under hydrostatic compression [17], and they provide three linear combinations of the TOECs [18]. Typically, stress derivatives of the second-order elastic constants under uniaxial stress loading augment the hydrostatic data to obtain the

full set of TOECs [19]. However, diamond's extreme stiffness and brittle behavior under uniaxial stress loading have precluded such measurements. To date, the TOECs of diamond have been estimated from a combination of available experimental data, theoretical models [20–22], and *ab initio* simulations [23]. The constants determined from these theoretical methods show large variations, demonstrating the need for an experimental determination of these constants.

Shock wave compression provides a unique approach to obtain the required experimental data. We have measured the elastic response of diamond crystals shock compressed along three different orientations. Finite strain theory to third order [24] applied to the measured uniaxial strain response provides three additional linear combinations of TOECs. By using the shock data and the hydrostatic compression results [17], the complete set of TOECs can be determined entirely from experimental measurements as shown here.

Diamond samples in our experiments were type IIa single crystal plates 2.5–3 mm in diameter and 0.4–0.6 mm thick. The samples were cut and polished to an optical finish, with the normal of the large face oriented along the [100], [110], or [111] direction, and were verified to be within 3° of the indicated orientation by using Laue x-ray diffraction. The experimental configuration used in this study is identical to that used in our earlier work, and the details can be seen there [25]. Impactors were launched by using a powder gun or a two-stage gun to velocities ranging from 2.1 to 3.7 km/s to achieve the desired peak stresses. A detailed discussion of our experimental results, including inelastic deformation data, will be presented elsewhere. Here, we focus only on the nonlinear elastic response.

Particle velocity histories at the diamond-LiF interface and elastic shock wave arrival times were recorded by using a multipoint velocity interferometer system for any reflector [26]. In experiments where a two-wave or an elastic-inelastic response was observed, only the initial interface velocity jump corresponding to the elastic wave

was considered. The elastic shock wave velocities and the *in situ* particle velocity jumps for elastic compression, determined by using impedance matching techniques [25,27], are plotted in Fig. 1. The uncertainty in the elastic shock velocities and the particle velocity jumps is estimated to be ~1% [25,28]. Also shown in Fig. 1 are data from a recent laser shock study [11] and the calculated elastic response using various sets of TOECs obtained from different theoretical calculations [20–23]. The large scatter and errors bars in the laser shock data preclude their use for determining the elastic properties of diamond. Hence, no further discussion of the laser shock data is presented in this Letter.

Under uniaxial strain loading, particle velocity and shock velocity measurements provide the necessary information to determine the longitudinal stress, longitudinal strain, and density in the shocked state using the Rankine-Hugoniot jump conditions [27]. The finite strain theory can then be used to determine the value of elastic constants that relate the stress and strain for that particular state.

The longitudinal stress, expressed by using the finite strain theory to third order, is [29]

$$\sigma'_1 = \frac{\rho_0}{\rho}\left(C'_{11}\eta'_1 + \frac{1}{2}C'_{111}\eta'^2_1\right), \qquad (1)$$

where ρ_0 is the initial density, ρ is the density of the shocked state, C'_{11} and C'_{111} are the second- and third-order isentropic longitudinal elastic constants, respectively, and η'_1 is the longitudinal Lagrangian strain. A prime indicates that the variable expressed is in the coordinate system aligned along the direction of shock wave propagation, namely, the [100], [110], or [111] direction. Appropriate tensor transformations relate the primed quantities to the crystallographic coordinate system.

For each of the orientations, the primed or effective TOECs are determined from least-squares fits of Eq. (1) to the experimental data, in conjunction with the published values for the second-order constants [17]; the latter are

well established. Given the destructive nature of our experiments, it was not feasible to conduct a sufficient number of experiments to obtain a statistically significant measure of the uncertainty solely from the fitting routine. Therefore, the uncertainties in the effective TOECs were conservatively estimated as the quadrature sum of the variation of the TOECs due to the experimental uncertainty and 2 standard deviations determined from the fitting routine. The results of the fitting routine and uncertainty analysis, and their relationship to the TOECs in the crystallographic (unprimed) coordinate system, are

$$C'^{[100]}_{111} = C_{111} = -7603 \pm 600 \text{ GPa}, \qquad (2)$$

$$C'^{[110]}_{111} = \tfrac{1}{4}(C_{111} + 3C_{112} + 12C_{166})$$
$$= -15\,146 \pm 1067 \text{ GPa}, \qquad (3)$$

and

$$C'^{[111]}_{111} = \tfrac{1}{9}(C_{111} + 6C_{112} + 2C_{123} + 12C_{144}$$
$$+ 24C_{166} + 16C_{456})$$
$$= -14\,631 \pm 1183 \text{ GPa}. \qquad (4)$$

The hydrostatic pressure derivatives of the second-order elastic constants of diamond [17] provide data to calculate three linear combinations of mixed isothermal-isentropic, third-order elastic constants [18]. The difference between the isentropic and mixed TOECs [30] was found to be very small (< 0.1 GPa) and was neglected in further calculations. Although the pressure derivatives [17] show sizable uncertainties (10%–20%) and were determined from data measured over a limited pressure range (~ 1.3 kbar) [17], the resulting linear combinations of TOECs determined from them are of comparable accuracy to the shock wave results. Together, the shock wave and hydrostatic compression measurements provide the six independent, linear equations from which all of the TOECs were determined.
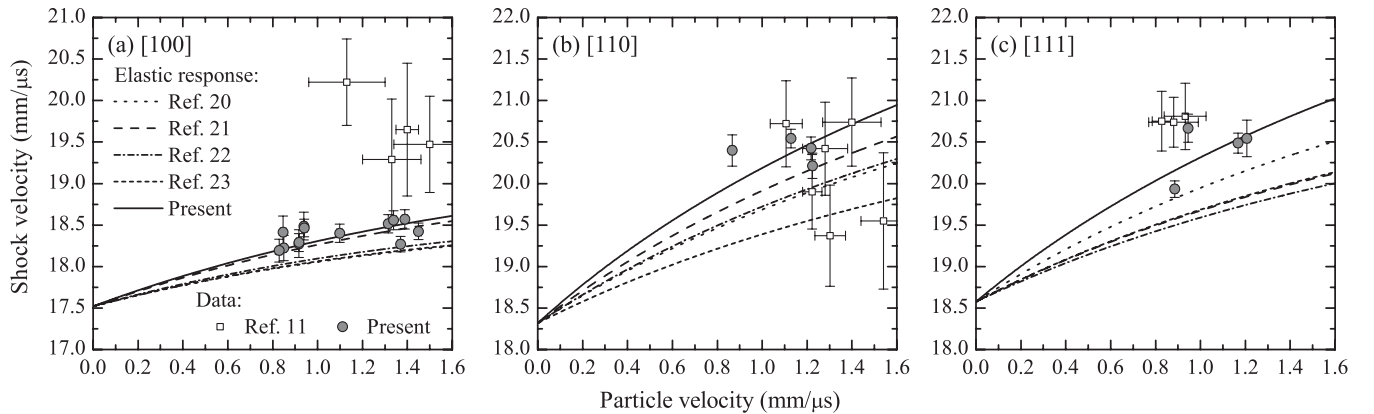

FIG. 1.   Elastic shock velocity and particle velocity measurements and calculated values using various sets of third-order elastic constants, for shock compression along (a) [100], (b) [110], and (c) [111].

TABLE I.   Third-order elastic stiffness constants of diamond in GPa.

	Ref. [20][a]	Ref. [21][a]	Ref. [22][a]	Ref. [23][b]	Present
C_{111}	-6260	-7367	-6475	-6300 ± 300	-7603 ± 600
C_{112}	-2260	-2136	-1947	-800 ± 100	-1909 ± 554
C_{123}	112	1040	982	0 ± 400	835 ± 1447
C_{144}	-674	186	115	0 ± 300	1438 ± 853
C_{166}	-2860	-3292	-2998	-2600 ± 100	-3938 ± 375
C_{456}	-823	76	-135	-1300 ± 100	-2316 ± 743

[a]These values were obtained from a combination of theoretical models and experimental data.
[b]These values were obtained from *ab initio* simulations at 0 K.

The complete set of our experimentally determined TOECs is tabulated in Table I along with previously reported sets of TOECs estimated from a combination of theoretical and experimental results [20–23]. The uncertainties in our set were determined by using standard methods of error analysis [28] from the uncertainties in the measured quantities. Except for C_{144} and C_{456}, the values reported in Ref. [21] are in reasonable agreement with our values. In general, the previously reported values [20–23] show significant variations with each other and with our results. These variations cast doubt on the adequacy of these theoretical models for describing the anharmonicity of diamond. Our work demonstrates the need for improvements to current theoretical approaches. A recent *ab initio* approach [31] has provided second- and third-order elastic constants for a cubic crystal (silicon) and a trigonal crystal (quartz) which are in reasonable agreement with experimentally determined values. Whether this approach [31] will result in better agreement with our measurements will be addressed at a future date.

Figure 2 shows the measured longitudinal stress-density compression data and the calculated elastic curves obtained by using the present set of TOECs and the previously reported sets [20–23]. The elastic response calculated by using only the second-order elastic constants is also shown. The results in Fig. 2 lead to the following conclusions. TOECs are required to match the measured nonlinear elastic response of diamond crystals, showing that lattice anharmonicity contributes significantly at large compressions. The differences between the different curves shown in Fig. 2 are smallest for the [100] orientation; this is not entirely surprising because C_{111} values (Table I) are generally comparable. For the other two orientations, the differences are larger because the other constants, which show larger variations, contribute to the nonlinear elastic response. The variations in the calculated longitudinal stress-density curves in Fig. 2 reflect the relative contributions of the TOECs that make up the effective longitudinal moduli indicated in Eqs. (2)–(4). Theoretically calculated curves for crystal orientations other than those examined in the present work can show large deviations from the measured values if they have significant contributions from TOECs which differ measurably from the experimental values. The longitudinal stress-density compression relations which fit our experimental results (solid lines in Fig. 2) are

$$\sigma_1'^{[100]} = 1079\mu + 984\mu^2 - 6665\mu^3 \text{ GPa}, \quad (5)$$

$$\sigma_1'^{[110]} = 1180\mu + 4356\mu^2 - 16\,776\mu^3 \text{ GPa}, \quad (6)$$

and

$$\sigma_1'^{[111]} = 1213\mu + 4026\mu^2 - 15\,940\mu^3 \text{ GPa}, \quad (7)$$

where $\mu = \rho/\rho_0 - 1$ is the density compression.
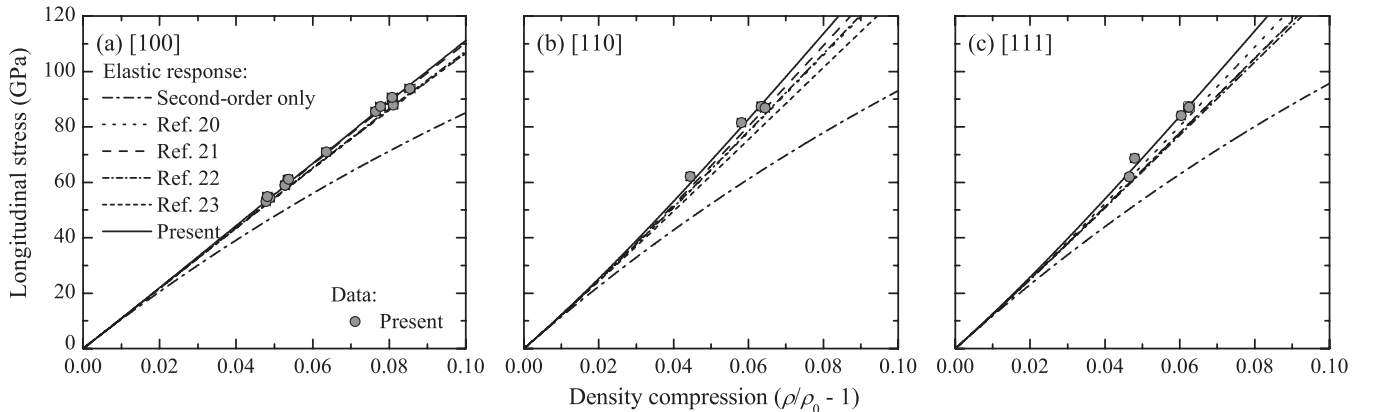

FIG. 2.   Calculated and measured elastic response of diamond shock compressed along (a) [100], (b) [110], and (c) [111].

The complete set of third-order elastic presented here addresses a long-standing scientific need to better understand the anharmonic and anisotropic response of diamond crystals. Refinements to theoretical models to match our results will provide better insight into the bonding and lattice response of carbon under extreme conditions. Anharmonicity plays an important role in the onset of solid-solid phase transitions, and our results provide a key starting point for understanding the high pressure solid-solid phase transition of diamond [10,12]. Knowledge of lattice anharmonicity and anisotropy is essential to characterize of the complex stress-strain states in the diamond anvils, increasing the utility of the Raman spectra of diamond as a pressure standard [8]. Our results are also expected to be useful for research on carbon in planetary astrophysics, fusion energy, and nanotechnology.

---

[1] M. Ross, Nature (London) **292**, 435 (1981).

[2] W. B. Hubbard, Science **214**, 145 (1981).

[3] L. R. Benedetti et al., Science **286**, 100 (1999).

[4] J. D. Lindl, *Inertial Confinement Fusion, The Quest for Ignition and Energy Gain Using Indirect Drive* (Springer, New York, 1998).

[5] X. Jiang et al., Diam. Relat. Mater. **19**, 21 (2010).

[6] J. E. Field, *The Properties of Natural and Synthetic Diamond* (Academic, San Diego, 1992).

[7] P. Loubeyre, F. Occelli, and R. LeToullec, Nature (London) **416**, 613 (2002).

[8] N. Dubrovinskaia et al., Appl. Phys. Lett. **97**, 251903 (2010).

[9] D. K. Bradley et al., Phys. Rev. Lett. **93**, 195506 (2004).

[10] M. D. Knudson, M. P. Desjarlais and D. H. Dolan, Science **322**, 1822 (2008).

[11] R. S. McWilliams et al., Phys. Rev. B **81**, 014111 (2010).

[12] D. K. Bradley et al., Phys. Rev. Lett. **102**, 075503 (2009).

[13] B. P. Barua and S. K. Sinha, J. Appl. Phys. **49**, 3967 (1978).

[14] S. Chantasiriwan and F. Milstein, Phys. Rev. B **58**, 5996 (1998).

[15] S. P. Łepkowski, Phys. Rev. B **78**, 153307 (2008).

[16] D. C. Wallace in *Solid State Physics*, edited by F. Seitz and D. Turnbull (Academic, New York, 1970), Vol. 25, p. 301.

[17] H. J. McSkimin and P. Andreatch, Jr., J. Appl. Phys. **43**, 2944 (1972).

[18] R. N. Thurston and K. Brugger, Phys. Rev. **133**, A1604 (1964).

[19] H. J. McSkimin and P. Andreatch, Jr., J. Appl. Phys. **35**, 3312 (1964).

[20] M. H. Grimsditch, E. Anastassakis, and M. Cardona, Phys. Rev. B **18**, 901 (1978).

[21] E. Anastassakis, A. Cantarero, and M. Cardona, Phys. Rev. B **41**, 7529 (1990).

[22] C. S. G. Cousins, Phys. Rev. B **67**, 024107 (2003).

[23] O. H. Nielsen, Phys. Rev. B **34**, 5808 (1986).

[24] R. N. Thurston, in *Physical Acoustics*, edited by W. P. Mason (Academic, New York, 1964), Vol. 1A, p. 1.

[25] J. M. Lang, Jr. and Y. M. Gupta, J. Appl. Phys. **107**, 113538 (2010).

[26] L. M. Barker and R. E. Hollenbach, J. Appl. Phys. **43**, 4669 (1972).

[27] R. G. McQueen et al., in *High-Velocity Impact Phenomena*, edited by R. Kinslow (Academic, New York, 1970), p. 293.

[28] J. R. Taylor, *An Introduction to Error Analysis* (University Science Books, Mill Valley, CA, 1982), p. 75, 2nd ed.

[29] J. M. Boteler and Y. M. Gupta, Phys. Rev. B **66**, 014107 (2002).

[30] K. Brugger, Phys. Rev. **133**, A1611 (1964).

[31] J. Zhao, J. M. Winey, and Y. M. Gupta, Phys. Rev. B **75**, 094105 (2007).